Analysis and Validation of Sensing Sensitivity of a Piezoresistive Pressure Sensor

Chih-Tang Peng[1], Ji-Cheng Lin[1], Chun-Te Lin[1], Kuo-Ning Chiang[2]

E-Mail: **Knchiang@pme.nthu.edu.tw**

Department of Power Mechanical Engineering

National Tsing Hua University

Hsin Chu, Taiwan 300, R.O.C.

Abstract

In this study, a packaged silicon based piezoresistive pressure sensor is designed, fabricated, and studied. A finite element method (FEM) is adopted for designing and optimizing the sensor performance. Thermal as well as pressure loading on the sensor is applied to make a comparison between experimental and simulation results. Furthermore, a method that transfers the simulation stress data into output voltage is proposed in this study, and the results indicate that the experimental result coincides with the simulation data. In order to achieve better sensor performance, a parametric analysis is performed to evaluate the system output sensitivity of the pressure sensor. The design parameters of the pressure sensor include membrane size/shape and the location of piezoresistor. The findings depict that proper selection of the membrane geometry and piezoresistor location can enhance the sensor sensitivity.

Keywords: Piezoresistive pressure sensor, Finite element method (FEM), Parametric analysis.

---

[1]. Graduate Assistant, Ph.D candidate

[2] . Corresponding Author, Associate Professor, Dept. of Power Mechanical Engineering, National Tsing Hua University

Ⅰ. Introduction

Since the discovery of piezoresistive effect, the applications of piezoresistive sensor are widely employed in mechanical signal sensing. The silicon based pressure sensor is one of the major applications of the piezoresistive sensor. Nowadays, silicon piezoresistive pressure sensor is a matured technology in industry and its measurement accuracy is more rigorous in many advanced applications.

The fundamental concept of piezoresistive effect is the change in resistivity of a material resulting from an applied stress. This effect in silicon material was first discovered by Smith [1] in the 1950's and was applied extensively in mechanical signal measurement for years. Smith proposed the change in conductivity under stress in bulk n-type material and designed an experiment to measure the longitudinal as well as transverse piezoresistance coefficients. Pfann [2] presented the shear piezoresistance effect, designed several types of semiconductor stress gauges to measure the longitudinal, transverse, shear stress and torque, and employed a Wheastone bridge type gauge in mechanical signal measurement. Piezoresistance coefficient is a function of impurity concentration and temperature; hence the thermal effect will influence the measurement result of a piezoresistive sensor. Kanda [3] produced a piezoresistance coefficient study about orientations, impurity concentration and temperature. Lund [4] also studied the temperature dependence of piezoresistance coefficient by four points bending experiment. The piezoresistive effect on polysilicon is another method to apply for mechanical signal sensing, French [5] presented the piezoresistive effect in polysilicon and its applications to strain gauges. In French's study, a comparison is made between theory and experiment for longitudinal and transverse strain measurements of n-type and p-type materials.

Piezoresistive pressure sensor design is widely studied at 1990's in MEMS and electronic packaging field. Jaeger et al. [6, 7] employed piezoresistive sensor made on silicon chip to measure the stresses within electronic packaging devices. Kanda [8] applied MEMS process to fabricate piezoresistive pressure sensors on {100} and {110} wafer for optimum design considerations.

Recently, the finite element method (FEM) is widely adopted for stress prediction, thermal effect reduction, packaging design and reliability enhancement of piezoresistive sensor. Pancewicz [9] used FEM to obtain the output voltage of the pressure sensor and compared the simulation data with experiment result. Schilling [10] also applied FEM analysis for sensor performance simulation and discussed the packaging effects on silicon piezoresistive pressure sensors. However, some design parameters such as packaging material and packaging structure that could influence the sensor stability were not discussed.

In this research, a comparison between experiment and FEA is accomplished. In the case study, the FEA demonstrated a promising result for the prediction of sensor performance. For the optimum design of sensor sensitivity, the FEA is adopted for the sensor performance design. The design parameters of the pressure sensor include membrane size/shape and piezoresistor location.

Ⅱ. Theory

- Fundamental theory of piezoresistance:

For a three-dimensional anisotropic crystal, the electric field vector (E) is related to the current vector (i) by a three-by-three resistivity tensor (ρ). The nine resistivity coefficients could be reduced to six and become a symmetrical matrix:

$$\begin{bmatrix} E_1 \\ E_2 \\ E_3 \end{bmatrix} = \begin{bmatrix} \rho_1 & \rho_6 & \rho_5 \\ \rho_6 & \rho_2 & \rho_4 \\ \rho_5 & \rho_4 & \rho_3 \end{bmatrix} \begin{bmatrix} i_1 \\ i_2 \\ i_3 \end{bmatrix} \tag{1}$$

The change in resistivity in the isotropic silicon can be obtained as follows:

$$\begin{bmatrix}\rho_1\\ \rho_2\\ \rho_3\\ \rho_4\\ \rho_5\\ \rho_6\end{bmatrix}=\begin{bmatrix}\rho\\ \rho\\ \rho\\ 0\\ 0\\ 0\end{bmatrix}+\begin{bmatrix}\Delta\rho_1\\ \Delta\rho_2\\ \Delta\rho_3\\ \Delta\rho_4\\ \Delta\rho_5\\ \Delta\rho_6\end{bmatrix} \tag{2}$$

Where $\Delta\rho$ is the resistivity change.

Based on the mechanics theory definition, the stresses are defined as six components: three normal stresses σ_x, σ_y, and σ_z, along the cubic crystal axis, and three shear stresses τ_{xy}, τ_{yz}, and τ_{xz}. To obtain the relation between resistivity and stresses, the piezoresistance coefficients π_{ij} (expressed in Pa^{-1}) are defined as a six by six matrix. For the cubic crystal structure of silicon, due to the symmetry conditions, the coefficients of matrix can reduce to three independent components: π_{11}, π_{12}, and π_{44}. Equation (3) depicts the relation of resistivity variations and stress as:

$$\frac{1}{\rho}\begin{bmatrix}\Delta\rho_1\\ \Delta\rho_2\\ \Delta\rho_3\\ \Delta\rho_4\\ \Delta\rho_5\\ \Delta\rho_6\end{bmatrix}=\begin{bmatrix}\pi_{11} & \pi_{12} & \pi_{12} & 0 & 0 & 0\\ \pi_{12} & \pi_{11} & \pi_{12} & 0 & 0 & 0\\ \pi_{12} & \pi_{12} & \pi_{11} & 0 & 0 & 0\\ 0 & 0 & 0 & \pi_{44} & 0 & 0\\ 0 & 0 & 0 & 0 & \pi_{44} & 0\\ 0 & 0 & 0 & 0 & 0 & \pi_{44}\end{bmatrix}\begin{bmatrix}\sigma_x\\ \sigma_y\\ \sigma_z\\ \tau_{yz}\\ \tau_{xz}\\ \tau_{xy}\end{bmatrix} \tag{3}$$

Combining equations 1, 2, and 3, the electric field in a cubic crystal lattice under stress is obtained:

$$\begin{aligned}E_1 &= \rho i_1 + \rho\pi_{11}\sigma_x i_1 + \rho\pi_{12}(\sigma_y+\sigma_z)i_1 + \rho\pi_{44}(i_2\tau_{xy}+i_3\tau_{xz})\\ E_2 &= \rho i_2 + \rho\pi_{11}\sigma_y i_2 + \rho\pi_{12}(\sigma_x+\sigma_z)i_2 + \rho\pi_{44}(i_1\tau_{xy}+i_3\tau_{yz})\\ E_3 &= \rho i_3 + \rho\pi_{11}\sigma_z i_3 + \rho\pi_{12}(\sigma_x+\sigma_y)i_3 + \rho\pi_{44}(i_1\tau_{xz}+i_2\tau_{yz})\end{aligned} \tag{4}$$

In order to derive the stress and the electric field expressed in an arbitrary Cartesian system, the <100> axis should be transformed into the given coordinate system. Two Cartesian coordinate systems x'y'z' and xyz, these two systems are related by the direction cosines are considered.

Equation 5 defines the matrix a_{ij}. The transformation equations of the electronic field (E), current (i), resitivity (ρ), stress (σ), and resistance coefficient (π) are given as the following equations:

$$\left[a_{ij}\right]=\begin{bmatrix} l_1 & m_1 & n_1 \\ l_2 & m_2 & n_2 \\ l_3 & m_3 & n_3 \end{bmatrix} \tag{5}$$

where $a_{ij} = \cos\left(x_i', x_j'\right)$

$$E_i^{'} = a_{ij}E_j \tag{6}$$

$$i_i^{'} = a_{ij}i_j \tag{7}$$

$$\rho_{ij}^{'} = a_{ik}a_{jl}\rho_{kl} \tag{8}$$

$$\sigma_{ij}^{'} = a_{ik}a_{jl}\sigma_{kl} \tag{9}$$

$$\pi_{ijkl}^{'} = a_{im}a_{jn}a_{ko}a_{lp}\pi_{mnop} \tag{10}$$

where

$$\left[a_{ik}a_{jl}\right]=\begin{bmatrix} l_1^2 & m_1^2 & n_1^2 & 2l_1n_1 & 2m_1n_1 & 2l_1m_1 \\ l_2^2 & m_2^2 & n_2^2 & 2l_2n_2 & 2m_2n_2 & 2l_2m_2 \\ l_3^2 & m_3^2 & n_3^2 & 2l_3n_3 & 2m_3n_3 & 2l_3m_3 \\ l_1l_3 & m_1m_3 & n_1n_3 & (l_1n_3+l_3n_1) & (m_1n_3+m_3n_1) & (l_1m_3+l_3m_1) \\ l_2l_3 & m_2m_3 & n_2n_3 & (l_2n_3+l_3n_2) & (m_2n_3+m_3n_2) & (l_2m_3+l_3m_2) \\ l_1l_2 & m_1m_2 & n_1n_2 & (l_1n_2+l_2n_1) & (m_1n_2+m_2n_1) & (l_1m_2+l_2m_1) \end{bmatrix}$$

For a membrane type piezoresistance pressure sensor, the stress state on the resistors can be assumed

to plane stress ($\sigma_z=\sigma_{xz}=\sigma_{yz}=0$) condition. After the transformation equations 5 to 10 are applied to equation 4, the equations are:

$$\begin{aligned} E_1'/\rho &= i_1'\left[1+\pi_{11}'\sigma_x'+\pi_{12}'\sigma_y'\right]+i_2'\left[\pi_{11}'\sigma_x'+\pi_{12}'\sigma_y'\right] \\ E_2'/\rho &= i_1'\left[\pi_{11}'\sigma_x'+\pi_{12}'\sigma_y'\right]+i_2'\left[1+\pi_{21}'\sigma_x'+\pi_{11}'\sigma_y'\right] \\ E_3'/\rho &= i_3' \end{aligned} \tag{11}$$

When the current and electronic field are both directed along the resistor axis, from the equations 1 and 11, the resistivity variation ratio is given by:

$$\Delta\rho/\rho = \pi_{11}'\sigma_x'+\pi_{12}'\sigma_y' \tag{13}$$

Because of the complexity of the equations, the longitudinal and transverse piezoresistance coefficients are defined as follows:

$$\pi_l = \pi_{11}' = \pi_{11}+2(\pi_{44}+\pi_{12}-\pi_{11})(l_1^2m_1^2+l_1^2n_1^2+m_1^2n_1^2) \tag{14}$$

$$\pi_t = \pi_{12}' = \pi_{12}-(\pi_{44}+\pi_{12}-\pi_{11})(l_1^2l_2^2+m_1^2m_2^2+n_1^2n_2^2) \tag{15}$$

From equations 13, 14 and 15, the resistivity variation ratio to a state of plane stress with a longitudinal stress, σ_l and a transverse stress, σ_t is given by:

$$\Delta\rho/\rho = \pi_l\sigma_l+\pi_t\sigma_t \tag{16}$$

- Wheatstone bridge to piezoresistive sensor:

Figure 1 illustrates a membrane with four piezoresistors.

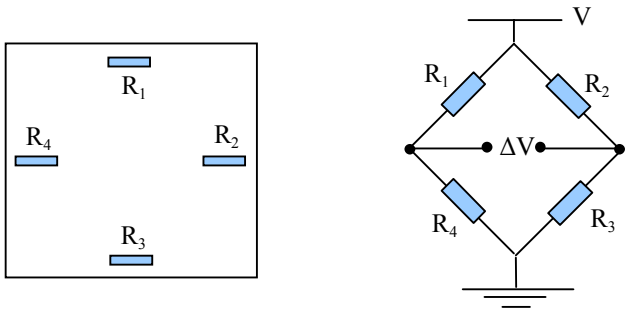

Fig. 1: Four piezoresistors on a membrane and Wheatstone bridge configuration of the four piezoresistors

Two resistors are oriented to sense stress in the direction of their current axis and two are placed to sense stress perpendicular to their current flow. The resistors are connected in a Wheatstone bridge (shown in Fig.1), where V is bridge-input voltage, and ΔV is differential output voltage. The resistance change due to unbalanced bridge can directly convert into a voltage signal under an applied pressure. Equation 17 shows the voltage and resistance relation:

$$\text{For } \Delta R \ll R,\ \frac{\Delta V}{V} = \frac{r}{(1+r)^2}\left(\frac{\Delta R_1}{R_1} - \frac{\Delta R_2}{R_2} + \frac{\Delta R_3}{R_3} - \frac{\Delta R_4}{R_4}\right) \tag{17}$$

$$r = \frac{R_2}{R_1} = \frac{R_3}{R_4}$$

Where ΔR_i is the i^{th} resistance change, R_i is the i^{th} zero-stress resistance.

- The relationship of stresses and output voltage:

The mechanical stresses obtained by FEA should be transferred into output voltage thus the simulation stress value can be applied to predict the equivalent output electrical signal. Equation 18 indicates the output voltage, resistance and stresses variation relation:

$$\frac{\Delta V}{V}=\frac{\Delta R}{R}=\frac{\pi_l(\sum_{i=1}^{n}\sigma_{li}\nu_i)+\pi_t(\sum_{i=1}^{n}\sigma_{ti}\nu_i)}{\sum_{i=1}^{n}\nu_i} \tag{18}$$

Where ΔV is differential output voltage, V is bridge-input voltage, ΔR is resistance changes, R is the zero-stress resistance, π_l and π_t are the longitudinal and transverse piezoresistance coefficients, respectively, i is the piezoresistive element number of finite element model, σ_{li} and σ_{ti} are, respectively, the longitudinal and transverse stresses of the i^{th} piezoresistive element, and ν_i is the volume of the i^{th} element on the piezoresistors. Figure 2 illustrates a quarter of finite element model. By applying this transfer method, the FEA simulation can be employed to predict the output signal of the piezoresistive pressure sensor.

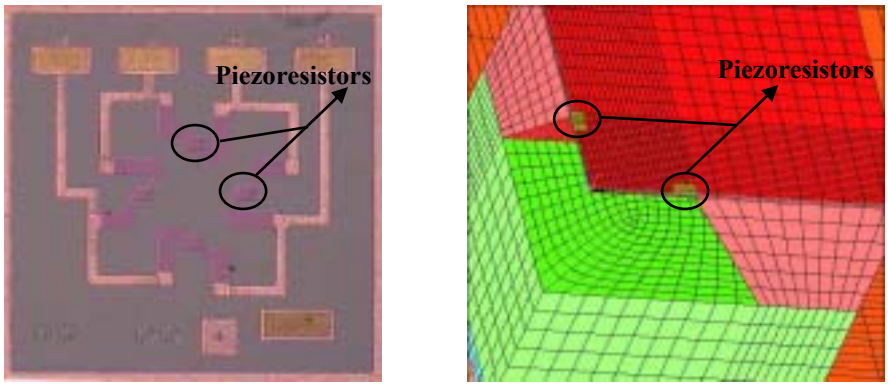

Fig. 2: Piezoresistors on the quarter of finite element model

Ⅲ. Comparison of finite element analysis and experimental results

In order to demonstrate the feasibility of the finite element analysis on sensor design, a prototype silicon base piezoresistive pressure sensor is fabricated and several pressures with thermal loading are applied on the sensor.

- Fabrication and experiment:

A piezoresistive pressure sensor is fabricated in this study. This sensor is fabricated by CMOS compatible process (except the anisotropic etching process) with six masks processing. A p-type

silicon wafer with <100> plane is used as a substrate for sensor fabrication. The piezoresistors connected in a Wheatstone bridge are located at (110) for longitudinal direction and $(1\bar{1}0)$ for transverse direction. Figure 4 illustrates the top view of the sensor.

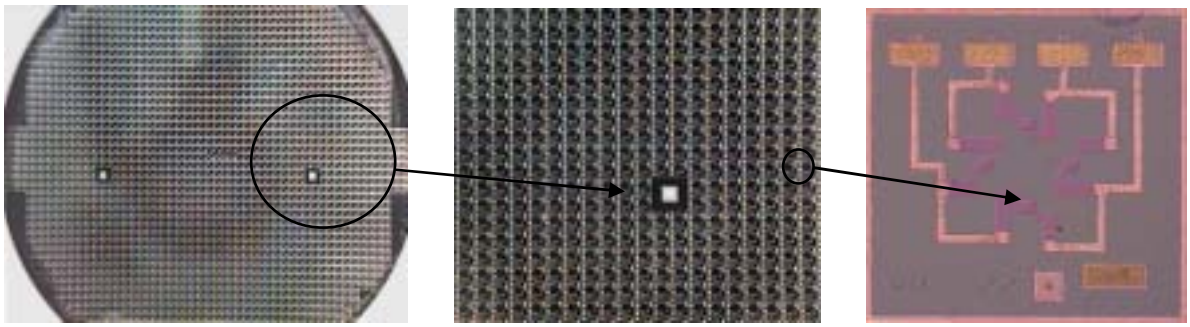

Fig. 4: Top view of a piezoresistive pressure sensor (bare die)

This pressure sensing device is composed of four parts: a PCB substrate, a glass substrate bonding with silicon, an adhesive layer between PCB and glass, and a membrane made by silicon with piezoresistive sensing units on it. Figure 5 illustrates the structure cross section and top view of this packaged pressure sensor. Table 2 indicates the dimensions of the fabricated sensor.

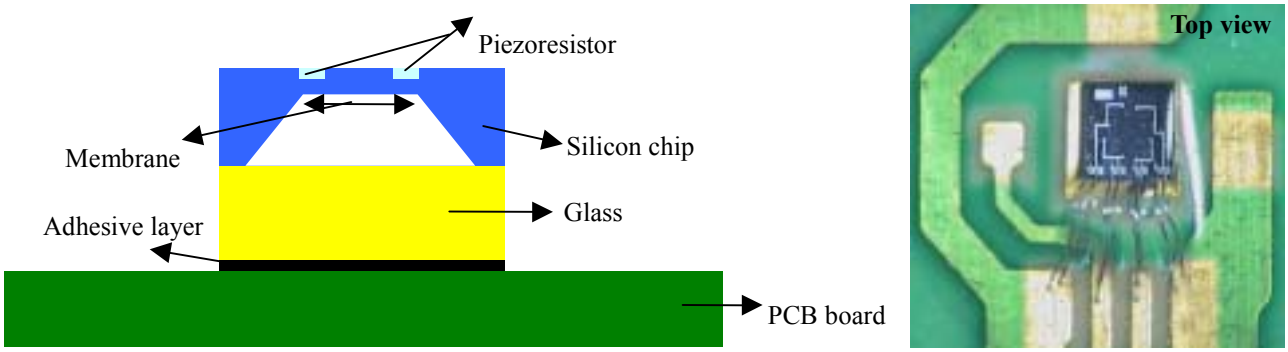

Fig. 5: The structure cross section and top view of the packaged pressure sensor

Table 2. Dimensions of PCB, glass, adhesive layer, silicon chip and silicon membrane

Layer	Length (μm)	Width (μm)	Thickness (μm)
PCB	10000	10000	1200
Glass	1800	1800	500
Adhesive	1800	1800	50
Silicon Chip	1800	1800	450
Silicon Membrane	600	600	20

The packaged pressure sensors are tested at 30psi and 40psi pressure loading with -10℃ to 60℃ environmental temperature conditions, and the input voltage is 5V. Figure 8 presents the measurement result.

- Finite element analysis:

In order to analyze and optimize the pressure sensor, the finite element analysis is employed to analyze the mechanical signal change due to thermal and pressure loading. In this study, the ANSYS finite element program is used. A three-dimensional eight-nodes element is adopted in this analysis.

A finite element model is established as a quarter model in Fig. 6, since the packaged pressure sensor device possesses quartered symmetry.

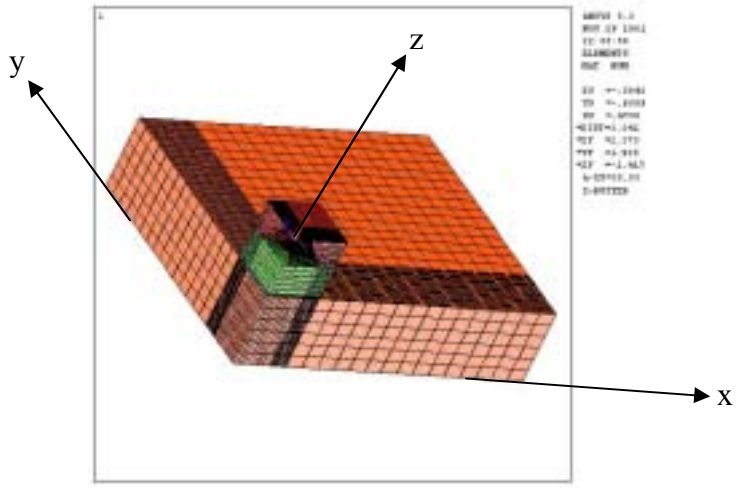

Fig. 6: One-quarter finite element model of piezoresistive pressure sensor

This finite element model contains 23,450 elements and 79,614 D.O.F. The boundary condition is with all nodes fixed in x, y, and z directions on the bottom side of PCB substrate and a symmetry condition is conducted on the xz and yz planes. The loading conditions are 30psi and 40psi pressure loading with the temperature of -10℃ to 60℃, and the stress free temperature is 25℃.

Table 3 indicates the material properties of PCB (FR-4), glass (7740), adhesive layer, and silicon.

Table 3. Material properties of PCB (FR-4), glass (7740), adhesive, and silicon

Layer	Young's Modulus (Gpa)	Poisson's Ratio	CTE (1/℃)
PCB (FR-4)	18	0.19	16ppm
Glass (7740)	76	0.28	3.25ppm
Adhesive	8.96	0.25	15ppm
Silicon	112.4	0.28	2.62ppm

In this study, owing to the piezoresistive coefficient as a function of temperature, the temperature coefficient of piezoresistor should be taken into consideration. Figure 7 presents piezoresistance factor which is influenced by temperature and impurity concentration for p-type silicon, where piezoresistance $\pi(N, T) = \pi_0 * P(N, T)$, N is the doping concentration, T is the temperature, π_0 is the piezoresistive coefficient at low-doped and room temperature condition and P(N, T) is the piezoresistance factor. A semiconductor fabrication process simulation software "TSUPREM" is applied in this work to obtain the doping concentration value of the piezoresistor.

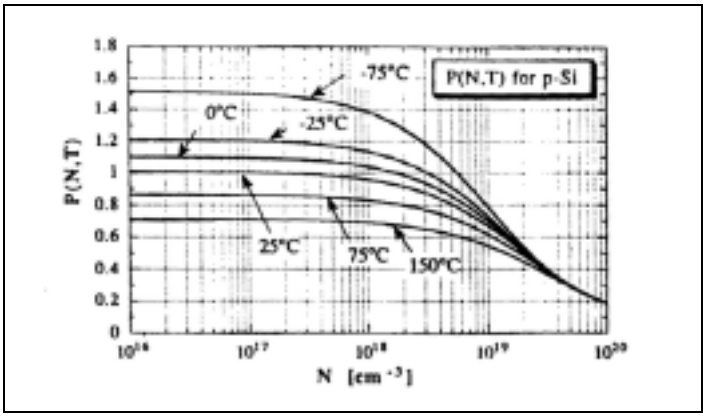

Fig. 7: Piezoresistance factor influenced by temperature and doping concentration (ref. [11])

The result of "TSUPREM" calculation shows that after annealing, the doping concentration value of the piezoresistor is $3.5*10^{18}(cm^{-3})$, hence the piezoresistance value that varies with temperature at this doping concentration can be applied in the simulation data.

The longitudinal and transverse piezoresistance coefficients of this sensor are $\pi_l = 1/2(\pi_{11}+\pi_{12}+\pi_{44})$ and $\pi_t = 1/2(\pi_{11}+\pi_{12}-\pi_{44})$, where $\pi_{11} = 6.6*10^{-11}$ (Pa^{-1}), $\pi_{12} = -1.1*10^{-11}$ (Pa^{-1}), and $\pi_{44} = 138.1*10^{-11}$ (Pa^{-1}) (p-type silicon at low doped value and room temperature condition, ref. [1]), respectively. The calculated longitudinal as well as transverse stresses are used to calculate the differential output

voltage.

Figure 8 presents the FEA simulation and experimental results. It is observed that the FEA gave a promising result with the experimental data, the average error between FEA and experiment is less than 3.5 %, thereby demonstrating that FEA can predict the mechanics signal output of the pressure sensor accurately. Based on the above validation, a parametric FEA method is applied to study the sensor performance and thermal as well as packaging effects of the pressure sensor.

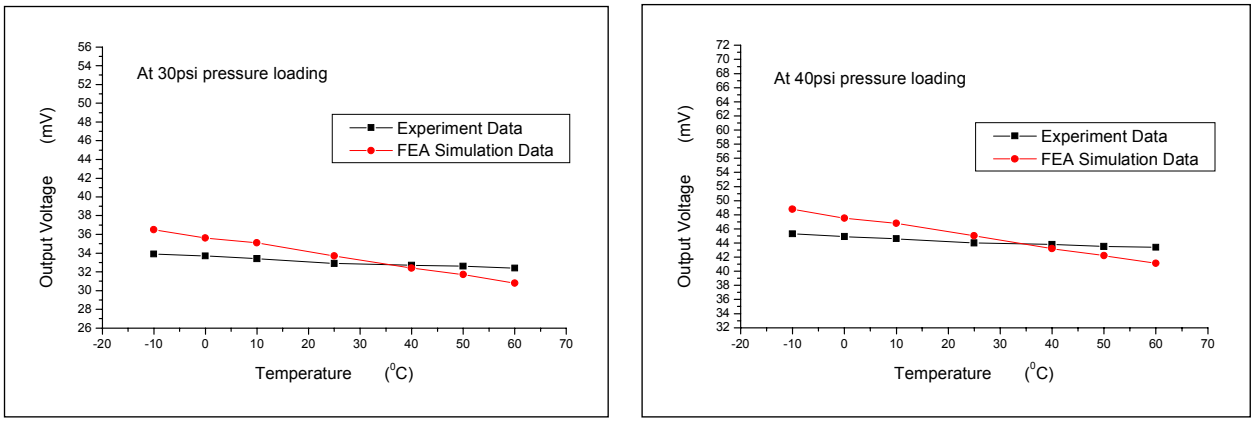

Fig. 8: FEA simulation and experiment data comparison result (at 30psi and 40psi)

Ⅳ. Parametric study for sensor sensitivity

The finite element analysis is employed to analyze the piezoresistive pressure sensor performance due to temperature and pressure loading with piezoresistor location and geometric structure of membrane. These parameters will influence the sensor sensitivity and stability. Table 3 indicates the material properties of PCB, glass (7740), adhesive layer and silicon. The boundary condition is the same as in Fig. 6. In these parametric studies, the applied pressure is 20psi, the temperature is from -10^0C to 60^0C, and the input voltage is 5V.

In this investigation, the parameters of the study include the location of piezoresistor, the shape of membrane, and the thickness of membrane. The locations of piezoresistor divided into five positions are illustrated in Fig. 9, the three shapes of silicon membrane are shown in Fig.10. The membrane sicknesses are 10μm and 20μm. The parametric study results are indicated as follows:

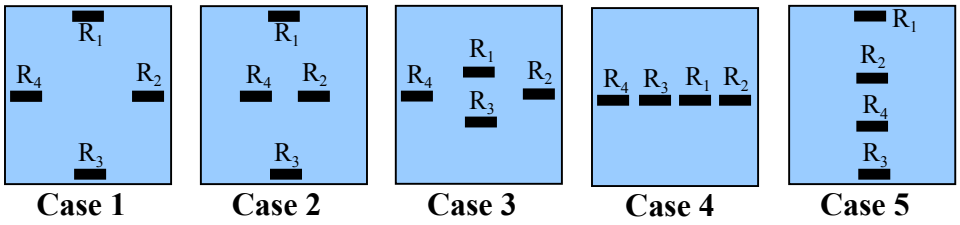

Fig. 9: The five locations of piezoresistors

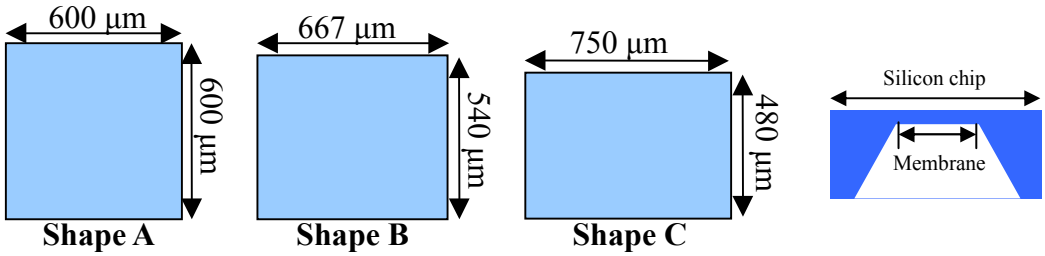

Fig.10: The three shapes of silicon membrane (with the same area but different shape)

A. The sensor sensitivity of the piezoresistor locations on membrane shape A

Different piezoresistor locations and silicon membrane shapes cause different sensor output voltages, a higher output voltage can enhance the sensor sensitivity and hence increases the sensor application range. Figure 11 illustrates the output voltage variation versus five piezoresistor locations on membrane shape A during different temperature loading. As shown in Fig. 11, in membrane shape A, case 1 shows the maximum output voltage and hence the piezoresistors at location1 has the highest sensitivity. Other locations of the piezoresistors (case 2 to case 5) do not show much difference between each other, and the output voltage of these locations are much lower than that of location 1. This phenomena is owing to the fact that the maximum stress (longitudinal and transverse stress) happen at the center of four sides of the membrane, and the piezoresistors of case 1 are all located in these locations, thereby case 1 shows the maximum output voltage. On the other hand, the stress at the center of the membrane distribute uniformly on membrane A, hence the output signal of the piezoresistors on these locations (case 2 to case 5) do not show much difference. Figure 12 indicates

the stress distribution of the membrane A.

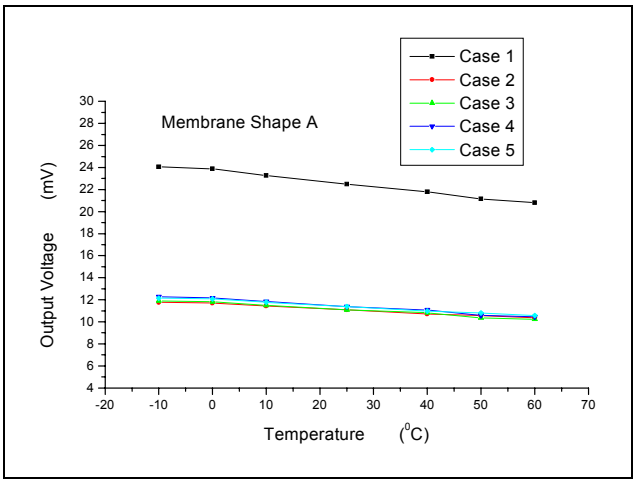

Fig.11: The output voltage variation versus five piezoresistor locations on membrane shape A

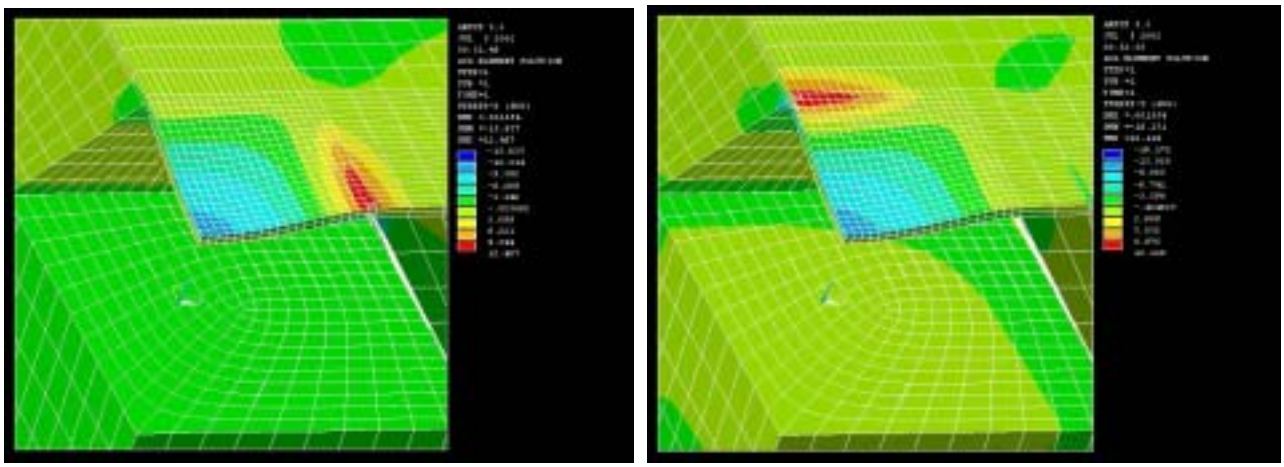

Fig. 12: The X and Y direction stresses distribution of membrane shape A at 60 ^{0}C

B. The sensor sensitivity of the piezoresistor locations on membrane shape B

Figure 13 illustrates the output voltage variation versus five piezoresistor locations on membrane shape B during different temperature loading. In Fig.13, on membrane shape B, location 1 still shows the highest sensitivity. But after comparing the stress distribution with membrane A, it could be seen

that the maximum X-direction stresses at the center of four sides on the membrane B decrease, the Y-direction stresses near the center of membrane increase and the X-direction stresses near the center of membrane decrease. Based on the above result, it could be explained why the output voltage of case 1 in membrane B is little lower than that in membrane A, and the output voltage of other piezoresistor locations in membrane B is higher than that in membrane A. In case 2 to case 5, the output signal of case 5 shows the largest increment. Figure 14 indicates the stress distribution of the membrane B.

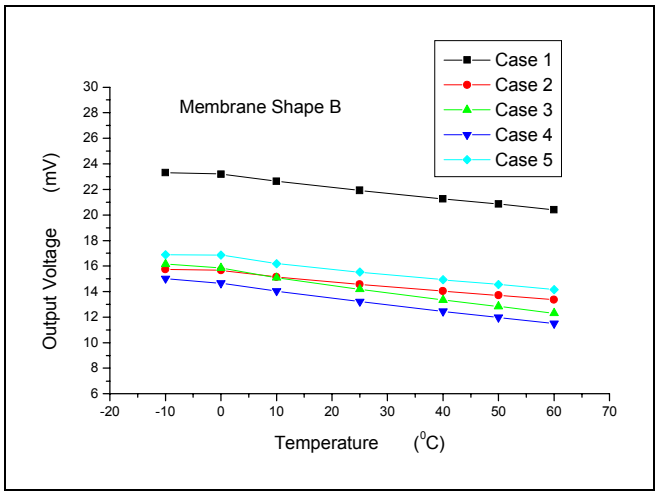

Fig.13: the output voltage variation versus five piezoresistor locations on membrane shape B

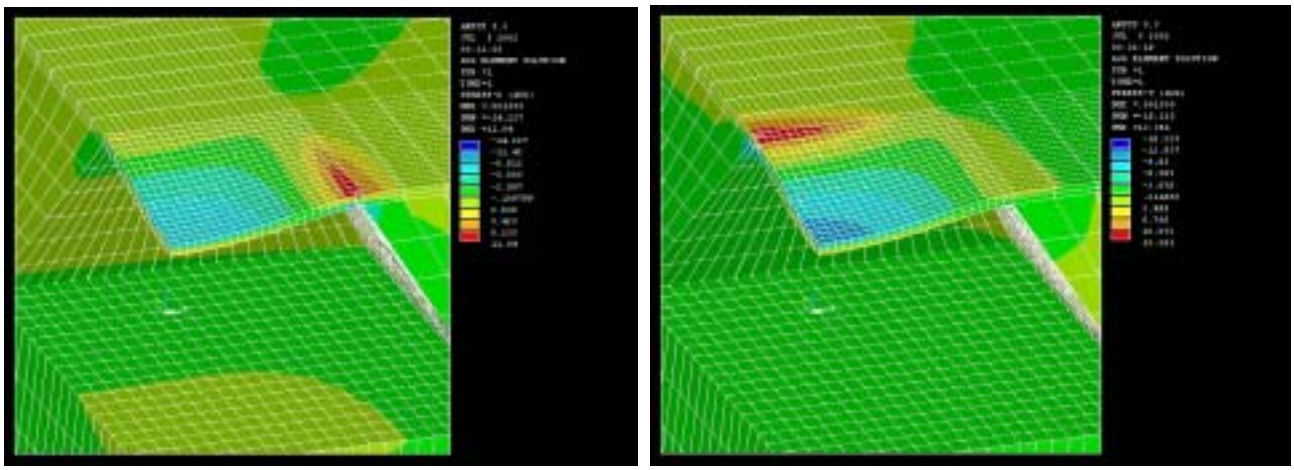

Fig. 14: The X and Y direction stresses distribution of membrane shape B at 60 ^{0}C

C. The sensor sensitivity of the piezoresistor locations on membrane shape C

Figure 15 illustrates the variation of output voltage with five piezoresistor locations on membrane shape C during different temperature loading. In membrane C, compared to membrane B, both the X-direction stresses at the center of four sides of the membrane and the X-direction stresses near the center of membrane are decreasing; thereby the output voltages of case 2 to case5 in membrane C are higher than that in membrane B and the output voltage of case 1 in membrane C is lower than that in membrane B. The output voltage difference between case 1 and case 5 in membrane C is much smaller than that in membrane B and membrane A. Figure 16 indicates the stress distribution of the membrane C.

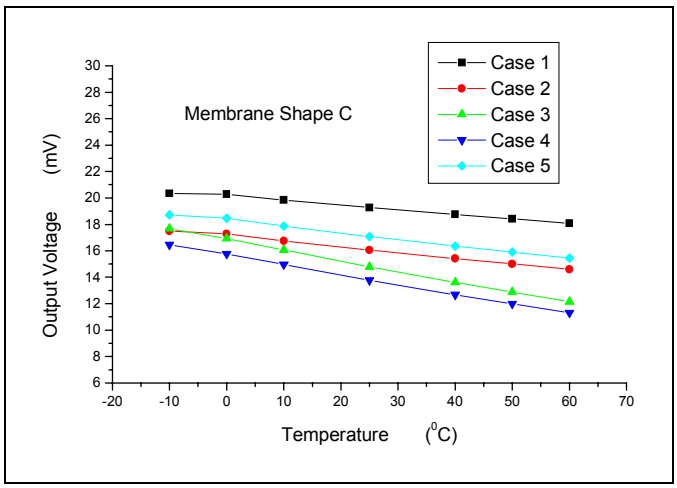

Fig.15: the output voltage variation versus five piezoresistor locations on membrane shape C

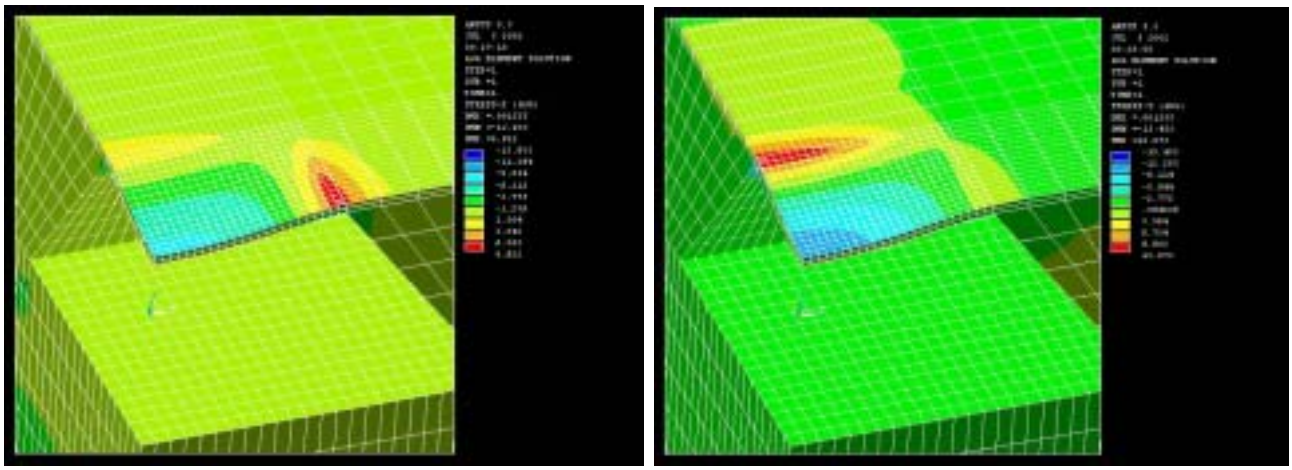

Fig. 16: The X and Y direction stresses distribution of membrane shape C at 60 ^{0}C

To conclude, the piezoresistor location of case 1 shows the best sensitivity in all three membranes. Although the membranes A, B and C are with the same membrane area, at location 1, the output voltage in membrane A shows the highest value. On the other hand, at location 5, membrane C shows the highest sensitivity among three membranes. Table 4 illustrates the comparison of output sensitivities of these three different membranes (with the same piezoresistor location).

Table 4: The output sensitivity comparison between three different membranes (with the same piezoresistor location)

	Case 1	**Case 2**	**Case 3**	**Case 4**	**Case 5**
Membrane A	Larger	Smaller	Smaller	Smaller	Smaller
Membrane B	Normal	Normal	Normal	Normal	Normal
Membrane C	Smaller	Larger	Larger	Larger	Larger

D. The membrane thickness effect

Figures 17 to 19 show the output voltage variation versus membrane thicknesses: 10 μm and 20 μm. No matter how the piezoresistor location is, these figures indicate that the output voltage increases as the membrane thickness decreases. Comparing the output sensitivity between 10 μm and 20 μm membrane thickness, the output voltage of 10 μm thick membrane is about 5 times to that of 20 μm thick membrane. It could be concluded that the thinner the silicon membrane, the higher the sensor sensitivity. On the other hand, the mechanical behavior of 10 μm thick membrane is similar to

that of 20 μ m thick membrane, thereby the output voltage at case 1 also shows the largest value and the output voltage at case 5 increases as well as the output voltage at case 1 decreases in turns of the membrane shape A, B and C.

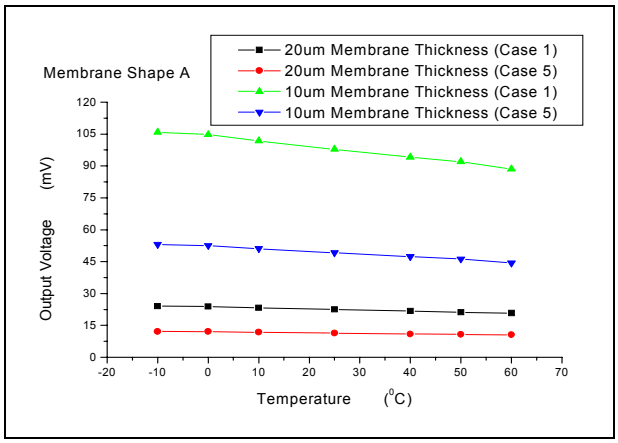

Fig.17: The output voltage variation of membrane A versus the membrane thickness

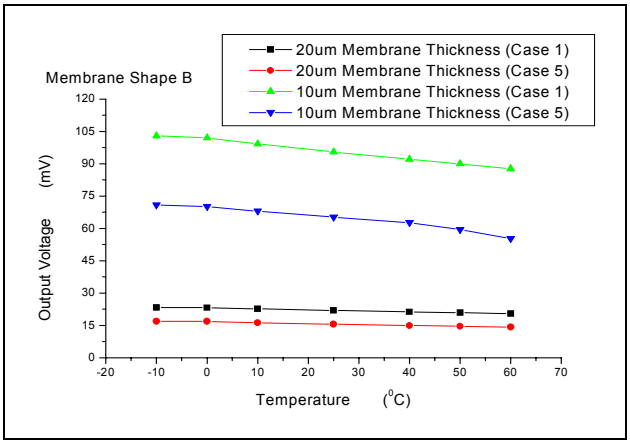

Fig.18: The output voltage variation of membrane B versus the membrane thickness

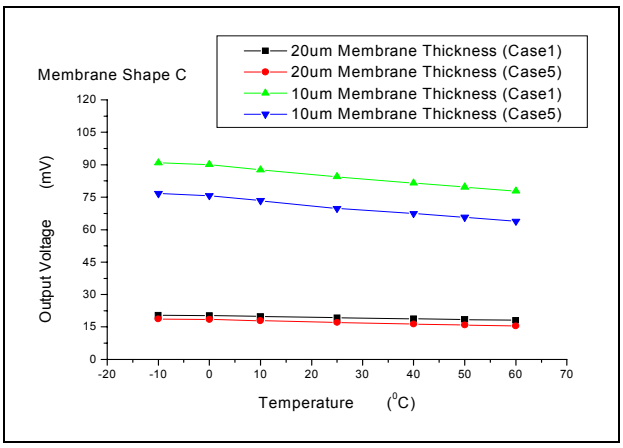

Fig.19: The output voltage variation of membrane C versus the membrane thickness

Ⅴ. Conclusion

In accordance with the well correlation between experimental and FEA results, the following conclusions are addressed:

1. The method proposed in this work for transferring the mechanical stresses of FEA data into output voltage is feasible, thus confirming that FEA can predict the external pressure loading behavior of the pressure sensor accurately, and it is a reliable tool for the sensor performance design.

2. According to the results of the parametric studies, it could be found that the thinner the silicon membrane, the higher the sensor sensitivity and the different piezoresistor locations show the different output sensitivities. The designer could depend on the system requirement to choose the membrane thickness and the piezoresistor locations.

References

[1] C.S. Smith, “Piezoresistance Effect in Germanium and Silicon”, Physical Review, Vol.94, pp.42-49, 1954.

[2] W.G. Pfann and R.N. Thurston, “Semiconducting Stress Transducers Utilizing the Transverse and Shear Piezoresistance Effects”, Journal of Applied Physics, Vol.32, pp. 2008 – 2018 , 1961.

[3] Y. Kanda, “A Graphical Representation of the Piezoresistance Coefficient in Silicon”, IEEE Transactions on Electron Devices, Vol. ED-29, No.1, pp.64-70, 1982.

[4] E. lund and T. Finstad, “Measurement of the Temperature Dependency of the Piezoresistance Coefficients in P-Type Silicon”, Advances in Electronic Packaging-ASME, EEP-Vol. 26-1, pp.215-218, 1999.

[5] P.J. French and A.G.R. Evans, “Piezoresistance in Polysilicon and Its Applications to Strain Gauges”, Solid-State Electronics, Vol.32, No.1, pp.1-10, 1989.

[6] R.C Jaeger, J.C Suhling, M.T Carey, and R.W Johnson, “A Piezoresistive Sensor Chip for Measurement of Stress in Electronic Packaging”, IEEE, pp.686-692, 1993.

[7] R.C Jaeger, J.C Suhling, A.T Bradley, and J.Xu, “Silicon Piezoresistive Stress Sensors Using MOS and Bipolar Transistors”, Advances in Electronic Packaging-ASME, EEP-Vol. 26-1, pp.219-225, 1999.

[8] Y. Kanda, “Optimum Design Considerations for Silicon Piezoresistive Pressure Sensor”, Sensor and Actuators, A62, pp.539-542, 1997.

[9] T. Pancewicz, R. Jachowicz, Z. Gniazdowski, Z. Azgin, P. Kowalski, “The Empirical Verification of the FEM Model of Semiconductor Pressure Sensor”, Sensor and Actuators, 76, pp.260-265, 1999.

[10] F. Schilling, W. Langheinrich, K. Weiblen and D. Arand, ”Simulation of Thermally Induced Package Effects with Regard to Piezoresistive Pressure Sensors”, Sensor and Actuators, A60, pp.37-39, 1997.

[11] S.M. Sze, “Semiconductor Sensors,” pp.173, John Wiley & Sons, 1994.